Influence of concrete strength and steel fibre geometry on the fibre/matrix interface

T. Simões[a,b], C. Octávio[a,b], J. Valença[a,b], H. Costa[a,c,*], D. Dias-da-Costa[d,e], E. Júlio[a,b]

[a]CERIS, Instituto Superior Técnico, Universidade de Lisboa, Portugal.

[b]Department of Civil Engineering, Architecture and Georesources, Instituto Superior Técnico, Universidade de Lisboa, Portugal.

[c]Department of Civil Engineering, Instituto Superior de Engenharia de Coimbra, Instituto Politécnico de Coimbra, Portugal.

[d]School of Civil Engineering, The University of Sydney, Australia.

[e]ISISE, Departamento de Engenharia Civil, Universidade de Coimbra, Portugal.

*Corresponding author; e-mail address: hcosta@mail.isec.pt

Keywords: fibre reinforced concrete; fibre type; fibre/matrix interface

Abstract

The main objective of the research described in this paper was to evaluate how the concrete compressive strength and the geometry of the steel fibres influence the behaviour of the fibre/matrix interface. With this aim, three different concrete matrices were designed with 20, 60 and 100 MPa, and two types of steel fibres were adopted (Dramix® 3D and Dramix® 5D). Specific pull-out specimens were produced and three sets of axial tensile tests were defined with different fibres (3D fibres, and 3D and 5D fibres with trimmed ends). A numerical model was calibrated and used to expand the scope of results obtained from the experimental tests. It can be concluded that the concrete compressive strength strongly influences the fibre/matrix strength. In the set with untrimmed 3D fibres, higher strengths are reached due to the hook shaped endings, for all concrete strengths, varying between 64% and 72% of the total load. For fibres with straight endings, increasing both diameter and length increases lead to higher adhesion and friction strengths.

1. Introduction

Fibre reinforced concrete (FRC) has recently experienced an increased interest, particularly in structures with high requirements for performance and durability. The behaviour of this type of concrete is mainly conditioned by the mechanical properties of both matrix and fibres, and also by the bond strength between the former and the latter's.

The inclusion of steel fibres in the concrete matrix leads to important changes in its behaviour, especially after cracking. FRC can experience a small increase in the cracking stress [1] and without significant change in stiffness up to that state [2]. After cracking, fibres resist to the applied load and the FRC shows much of its advantages compared with current concrete. Fibres bridge the cracked surfaces delaying the opening and providing stress transfer along the crack and allowing energy absorption by the FRC. This results in a failure type change, from brittle to ductile [3–5]. Thus, fibres crossing a crack in FRC can transfer internal forces [6], from the fibre to the matrix, by mobilizing adhesion and friction. The behaviour of the fibre/matrix interface is important to define the overall behaviour of this composite material, since it influences the strength magnitude and how the internal forces are transferred to the fibre matrix. This process may cause slipping and deformation of the fibre, but also its rupture if the bond strength is higher than the tensile strength of the fibre [7–9].

Studies on the fibre pull-out behaviour have been conducted, but only focusing the behaviour of a single fibre embedded in concrete [10]. The studies referred to in the next sentences reveal that there are several parameters that can influence the pull-out behaviour, namely: the adoption of hooks at the ends of the fibre, the geometry of the hooks, the orientation and embedded length of the fibre, and the strength of the matrix. Currently, the most widely used fibres in structural concrete industry, in terms of configuration, are either smooth or with hooks at the ends. The choice between these two types of fibres depends on the desired behaviour of the FRC [11]. The energy required to completely pull-out a fibre with a hooked end is usually higher compared to a straight fibre. For fibres with identical lengths and diameters, the energy is always higher in the presence of hooks. While smooth fibres resist pull-out essentially by adhesion, fibres with hooks at the ends present an additional mechanical strength. Thus, the latter requires more energy to deform the fibre and thereby to pull-out. Recent studies [9,12–14] suggest that fibres with a deformed shape specified by the manufacturer require more energy to pull-out than straight fibres. However, for recycled steel fibres the pull-out energy seems to be lower than that of straight fibres [15], even if having a deformed shape, due to the previous use and/or recycling process.

Regarding the fibre orientation, it may present different inclinations to the surface of the concrete, from perpendicular (0º with the pull-out axis) up to an inclination near 90º with the pull-out axis. However, for experimental testing the most acceptable inclinations ranges from 0 to 60º with the pull-out axis. The fibre inclination influences the failure mode of the fibre/matrix interface. Some studies [8,16–18] showed that by increasing the fibre inclination, the behaviour tends to change from slipping failure to failure of the fibre or to failure of the matrix combined with fibre pull-out. The embedded fibre length is also important since,

together with the fibre diameter, it defines the contact area between fibre and matrix. This contact area is where the frictional strength is developed and the majority of the studies [7,12,16] show that with the increase of the contact area, the bonding strength of the fibre/matrix interface also increases.

The strength of the matrix is a significant factor to the bond strength of fibre/matrix interface. The maximum shear stress ($\tau_{máx}$) defined by the *fib* Model Code 2010 [19] referring to pull-out of steel bars, clearly depends on the concrete compressive strength (f_{ck}), increasing for higher compressive strengths (for smooth surfaces, $\tau_{máx} = 1.25 \times \sqrt{f_{ck}}$). For steel fibres, some studies [7,8,12] suggested an increase in the pull-out strength with the increase of the matrix compressive strength.

As mentioned above, studies on the fibre pull-out behaviour have already been conducted, but only focusing the behaviour of a single fibre embedded in concrete. The study herein described aimed at evaluating the behaviour of fibre/matrix interface considering a bundle of single orientated fibres embedded in concrete. The influence of the following parameters was assessed:

- The compression strength of the matrix;
- The presence of hooks at the ends of the fibre;
- The diameter and the length of the fibre;

In addition, a constitutive model for the fibre/matrix interface was proposed for finite-element based software.

This paper is organised as follows: Section 1 synthesizes the conclusions of previous studies and presents the research significance of the present study. Section 2 describes the experimental programme, including material properties, specimens' geometry, and testing set-up. In Section 3, the main results are presented and the interface behaviour is discussed. Lastly, Section 4 presents the main conclusions of this research.

2. Materials and Methods

The experimental programme was defined by taking into account the aims previously listed. In this section, the material properties, the number and geometry of specimens, the test set-up, and the data acquisition systems are described.

2.1. Material properties

Three types of fibre reinforced cement matrix (FRCM) were designed as part of this research work, targeting different compressive strengths. The cement type was selected depending on the required performance of the mixture, namely CEM II/B-L 32.5N, CEM II/A-L 42.5R, and CEM I 52.5R were adopted for 20, 60 and 100 MPa compressive strength mixtures, respectively [20]. In addition, water, a third generation superplasticiser (eter-polycarboxylates based), classified as T3.1, T3.2 and T7 by EN 934-2 [21], and two types of siliceous sand – fine (0/1 mm) and medium (0/4 mm), with fineness modulus of 2.62 and 3.53 respectively – were also considered.

The mixtures were designed based on the Feret's expression to predict the strength of the binding paste as described in [22]. Both Feret's coefficient and air content were first determined in preliminary test mixtures, adjusting admixture dosage, until obtaining the predicted values. The mixtures were progressively corrected to the point that final formulations were reached, in which compressive strengths were close to the initially defined target. Table 1 shows the final composition of each mixture. The compressive strength tested at 28 days for the three concrete matrices were respectively 19.0, 64.3 and 100.4 MPa, being respectively named C20, C60 and C100. The Young's modulus was also measured according to E-397 standard [23], and the following values were recorded: 18.8, 24.2 and 29.7 GPa, respectively.

Specimens were produced using Dramix® 3D and Dramix® 5D steel fibres. The corresponding properties are presented in Table 2. It should be mentioned that in spite of the differences between fibres, namely diameter, length and tensile strength, the aspect ratio is similar for both.

Table 1 – Matrices final dosages (kg per cubic meter)

Mixtures	Constituents						
	CEM II/B-L 32.5R	CEM II/A-L 42.5R	CEM I 52.5R	BASF Glenium Sky 526	Water	Fine Sand	Medium Sand
C20	366.5	-	-	0.92	253.6	341.5	1148.8
C60	-	554.8	-	3.88	229.8	191.8	1257.7
C100	-	-	788.6	10.3	204.0	-	1335.8

Table 2 – Main properties of adopted fibres

Type of fibre	Diameter (mm)	Length (mm)	Young's modulus (GPa)	Tensile strength (MPa)
Dramix® 3D	0.55	35	210	1345
Dramix® 5D	0.90	60	210	2300

2.2. Specimens production

After the concrete dosages and the type of fibres were settled, the production of test specimens took place. These consist of two concrete cubes, with 10 cm edges and without adhesion to each other, only connected by a single orientated fibres bundle. The latter was previously embedded in a k-line square piece (Figure 1a) with the dimensions of the cubes' edge and coated with adhesive film. The smooth surface of the adhesive film prevented the adhesion between the two concrete cubes. The k-line piece, with the fibres bundle (16 fibres equally spaced between them) was then placed in a steel mould with the final dimensions of the specimen (Figure 1b) and concrete was cast simultaneously on both sides (Figure 1c). It should be noted that in each of the specimen's cubes, a steel bar was placed, to which the test tensile force would be applied. The specimens were removed from the formwork approximately 24 hours after casting and placed in a climate-controlled chamber. Finally, they were removed circa 24 hours before the tests.

(a) (b) (c)

Figure 1 – Specimens production: (a) placement of the fibres at the k-line sheet; (b) placement of the k-line sheet in the mould; and (c) concrete casting in the moulds.

With the above-mentioned specimens, three sets of tests were defined. In the first, named 3D1, one of the ends of the adopted fibres (Dramix® 3D) was cut off. As a result, in one of the concrete cubes, the fibre end was straight, forcing slippage on this side, being the embedded length of the fibres in the concrete of 13 mm. The second set, designated 5D1, was similar to the first, differing only in the type of fibre (Dramix® 5D) and the embedment length (23 mm). Finally, in the third set, designated 3D2, Dramix® 3D fibres were adopted intact, i.e., without cutting off any of the ends, and were placed in the k-line sheet, adopting identical embedment lengths in each concrete cube. In these sets, two specimens for each target strength of 20, 60 and 100 MPa were used for each situation.

2.3. Test set-up

The specimens were tested in tension at the age of 28 days. The load was applied by a hydraulic servo-actuator with a reading accuracy of 0.16% of the measured value, using displacement control, at a rate of 0.50 mm/min. This type of control has been selected instead of force control to allow the study of the pull/slip effect between fibres and the matrix. The instrumentation included four displacement transducers (1 to 4 in Figure 2) and a load cell. Two adjacent faces (1-2, between transducers 1 and 2; and 2-3, between transducers 2 and 3) of the specimens were also monitored through photogrammetry [24,25], allowing the displacement between faces to be measured. This was performed for the instant of 'maximum load' and the instant of 'maximum displacement', i.e., the displacement for which fibres were still equally mobilized (Figure 3a). In fact, during tests, it was observed a first phase where the differential displacements between the specimens' faces were almost null, suggesting that all fibres were experiencing identical strains. Then, a second phase where the differential displacements start to increase, suggesting an uneven mobilization of fibres. This second phase was discarded and the displacement between both phases was assumed as the 'maximum displacement'. The procedure consists in measuring the differences of the centres of circular targets, painted next to the interface in each part of the specimen, during the tests (Figure 3b and c). The coordinates of those centres were detected by applying an algorithm based on Hough transform [26]. Four

larger targets, placed outside the interface, were used to normalise and scale all images by applying homography transformation [24]. The monitoring set-up allowed a detailed assessment of the fibre/binding matrix interface, in particular the determination of the bonding strength and the characterisation of the post-peak response.

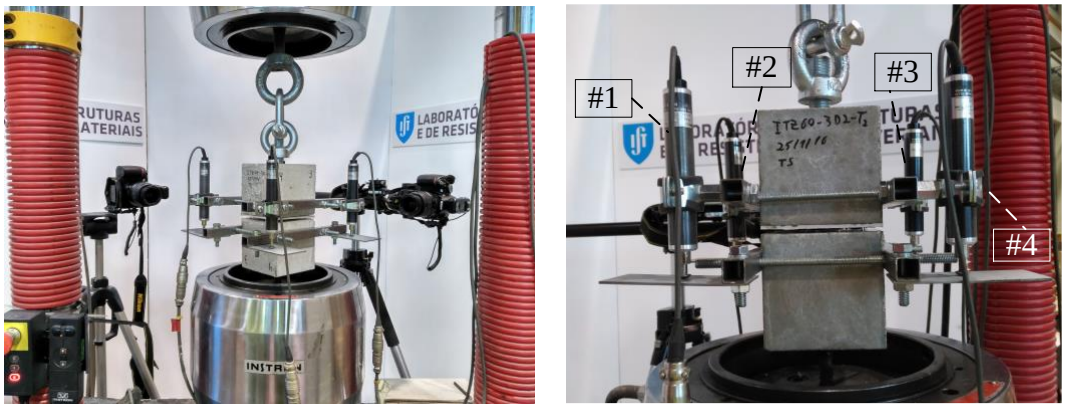

(a) (b)

Figure 2 – Test setup: (a) test with the various data acquisition systems; and (b) LVDT identification.

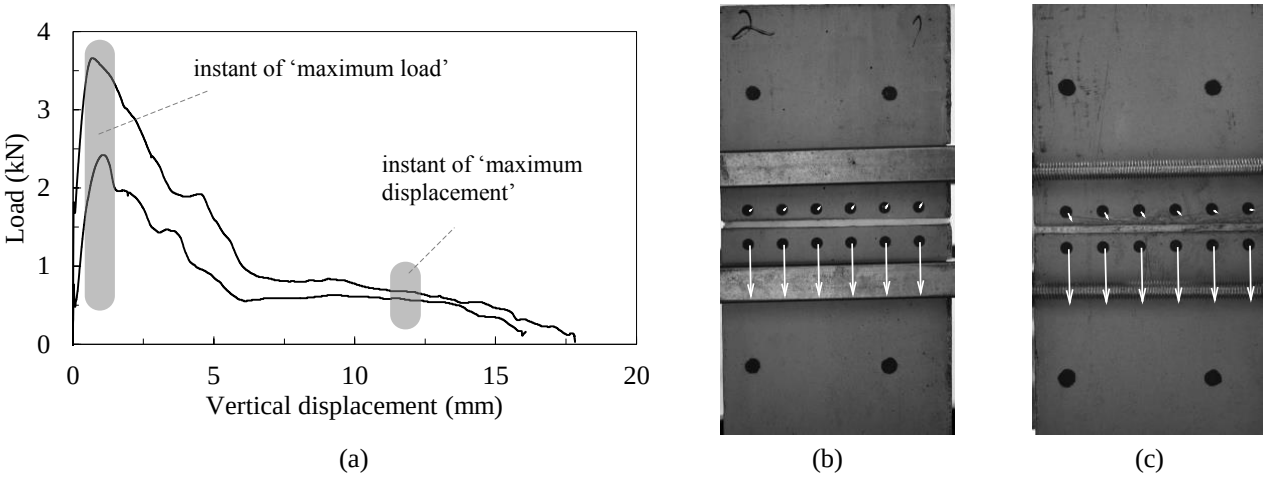

(a) (b) (c)

Figure 3 – Displacement assessment with photogrammetry: (a) analysed instants; (b) 1-2 face with final displacement vector; and (c) 2-3 face with final displacement.

3. Results and discussion

3.1. 3D1 set

Figure 4 shows the load-displacement curves and the comparison between the displacements obtained by photogrammetry between adjacent faces for the respective specimens of 3D1 test series. Figure 4b shows that after reaching the maximum load the displacement between adjacent faces becomes similar.

The analysis of the load-displacement curves of Figure 4a shows that the behaviour of specimens with C20 and C60 concretes exhibit two separate stages: the first in which there is a maximum peak load; and a second in which the load decreases and remains approximately constant. The samples produced with C100 concrete also show these two stages, but in this case, the load does not remain constant. On contrary, it gradually

decreases during the test, approaching the values obtained with the C60 concrete. The first stage until the peak load corresponds to the strength component given by the adhesion between matrix and fibres. At this stage, it is verified an increasing load for small displacements. The second stage corresponds to the strength component of the friction between the matrix and the fibres, starting from the instant in which there is relative movement at this interface. In the case of C20 concrete, frictional strength corresponds to approximately 30% of the adhesion strength, while in the case of C60 and C100 concretes, frictional strength corresponds to approximately 70% of the adhesion strength.

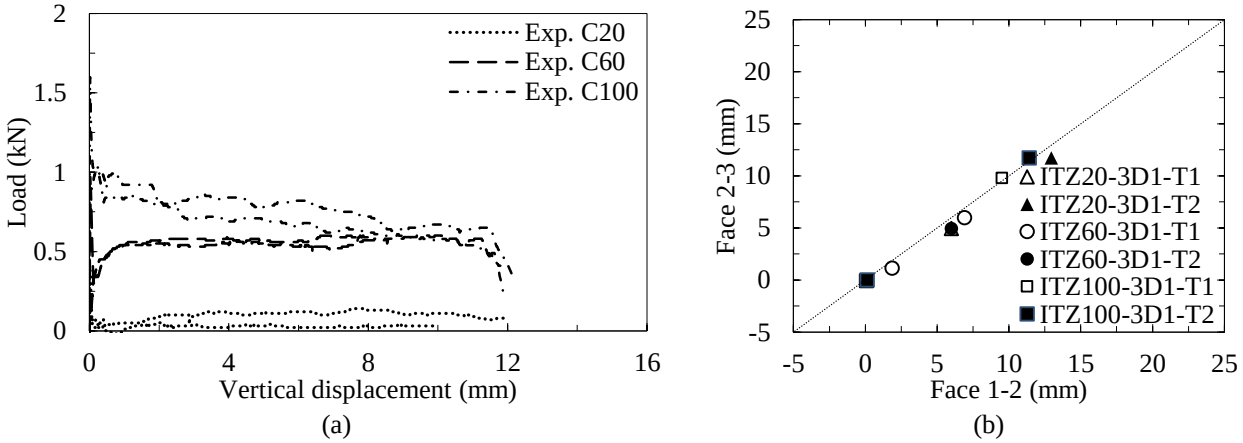

Figure 4 – 3D1 tests: (a) load-displacement curves; and (b) relative displacement between adjacent faces.

In Figure 5a the shear stress-slip relation in the fibre/matrix interface is presented and Figure 5b shows a schematic definition of slip. Since fibres responded in a first stage with no significant differential displacements between faces, slipping (s) was determined based on the longitudinal displacement (d) at the centre of the specimen by subtracting the elongation of the fibres (ΔL) calculated from the current applied load and Young's modulus of the fibres. This calculation was stopped when differential displacements started to take place. After some variations in the beginning of the test, the behaviour of all the sets follows the same trend: throughout the test as the fibre is progressively pulled out, and consequently less length is embedded in the matrix, the shear strength at the fibre/matrix interface increases. This may occur due to debris left in the contact area of the fibre/matrix interface caused by the pull-out of the fibres. The damage on the fibre surface can also increase its roughness and increase the friction stress. Regarding the concrete compressive strength, while this parameter rises, the referred shear strength is also higher, as suggested by the *fib* Model Code 2010 [19].

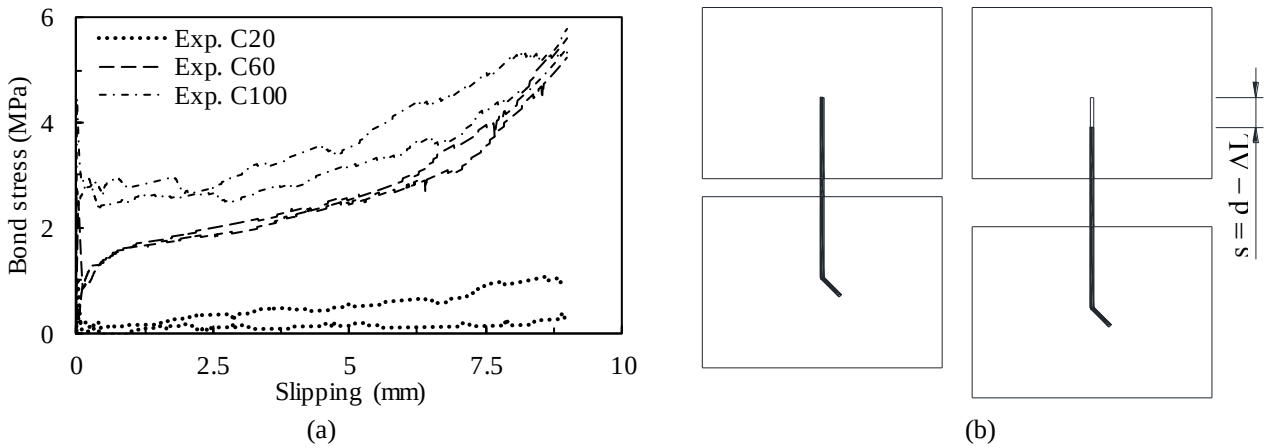

185 Figure 5 – (a) Bond stress-slipping curve for 3D1 tests; and (b) schematic definition of slip.

186 3.2. 5D1 set

187 Figure 6a represents the load-displacement curves of 5D1 series. Figure 6b, which shows the relative
188 displacement between adjacent faces of the specimens, reveals that after the initial instants of asymmetric
189 behaviour, the samples tend to have identical displacement on all sides.

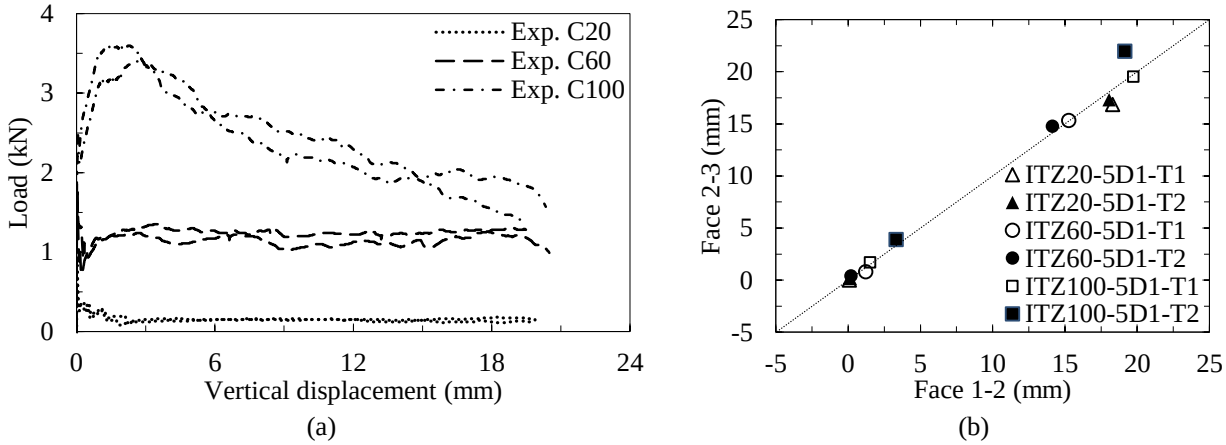

190 Figure 6 – 5D1 tests: (a) load-displacement curves; and (b) relative displacement between adjacent faces.
191

192 In the 5D1 set, the specimens produced with the C20 and C60 concretes showed an overall behaviour similar
193 to the corresponding 3D1 set specimens. However, in this case, the frictional strength component
194 corresponds to 30% and 70% of the adhesion strength to the specimens manufactured with C20 and C60
195 concretes, respectively. The specimens produced with C100 concrete, apparently show a distinct behaviour.
196 The first drop in the load corresponds to the failure of the adhesion component of bond. After this, the fibres
197 start to slip from the matrix and friction starts to develop. In this stage, the load increases and friction
198 becomes more significant than adhesion, mainly due to the suitable properties of the matrix, until the
199 maximum load is reached. After reaching the maximum load, in the second phase of the test, the strength
200 gradually decreases, as observed in the corresponding specimens of the 3D1 set. The frictional strength
201 component represents approximately 150% of the adhesion component.

Figure 7 shows the shear stress-slip relation in the fibre/matrix interface. The analysis of these curves suggests the conclusions abovementioned for the 3D1 set, which means that the shear strength is less influenced by the fibre diameter and more influenced by the fibre length, because of the higher strength for lower values of embedded fibre in the matrix. The bond stress of both tested set (3D1 and 5D1) are within the range proposed by *fib* [27], that suggests values between 1 and 10 MPa, depending on the type of fibre and concrete.

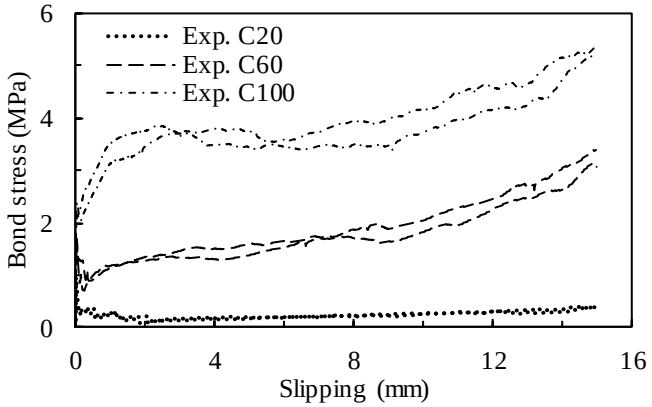

Figure 7 – 5D1 tests: bond stress-slipping curve

3.3. 3D2 set

Figure 8a shows the load-displacement curves for the 3D2 specimens and Figure 8b shows the ratio of displacement between the two faces monitored with photogrammetry. In this case, the relative displacements presented higher values and slip was not determined, since load and displacement were not similar for all fibres.

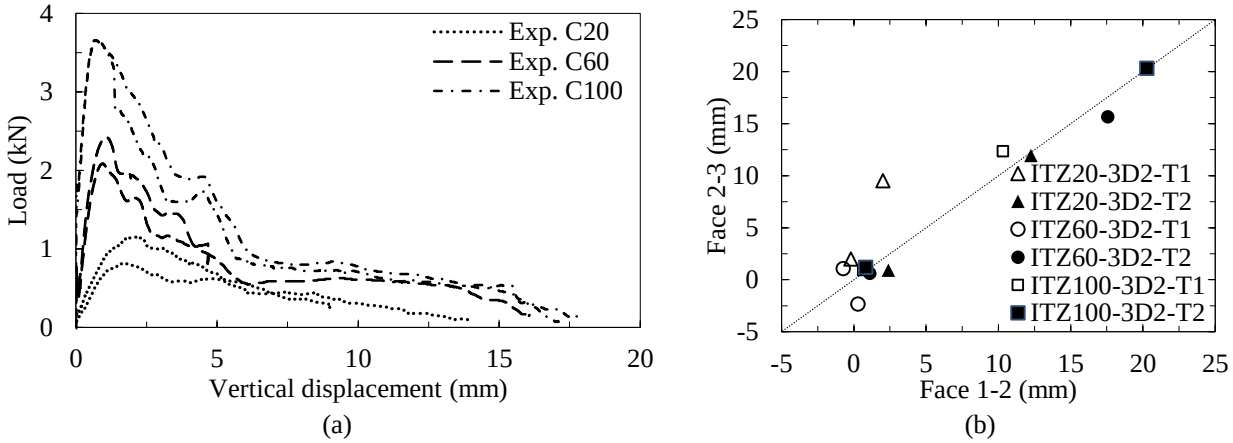

Figure 8 – 3D2 tests: (a) load-displacement curves; and (b) relative displacement between adjacent faces.

In 3D2 tests, where the fibres have been placed in its usual configuration (with no removal of one of the hooks), the general behaviour of the specimens was similar. In all the tests an increase of strength was observed up to the maximum peak, followed by a load decrease. In C20 specimens the load reaches a peak at a displacement of approximately 2 mm. After this instant, the load smoothly decreases, corresponding to the slipping of the fibre relatively to concrete, with the hooks already deformed. It is also relevant to mention

that, for the 3D2 specimens with C20 concrete, none of the fibres presented rupture. For the specimens produced with C60 and C100 concretes, the load reached a peak and then dropped abruptly. The maximum load was reached for smaller displacements with the increase in concrete strength. The sudden drop of the load after the peak is due to the rupture of fibres, which was more pronounced in the specimens produced with C100 concrete, which explains the sudden loss of strength in this case. It is noted that, after approximately 6/7 mm of displacement, the strength loss has become less significant, because beyond that, there is no fibre failure, being the strength achieved only by friction between the remaining fibres and concrete.

In order to improve the behaviour and the analysis of the bond strength components of the fibre/matrix interface, the average values of peak load and of the adhesion strength, for the tested situations, are presented in Table 3, depending on fibres and on matrix nominal strength.

Table 3 – Peak loads and adhesion strengths for all the sets.

Fibre	3D2			3D1			5D1		
Matrix strength (MPa)	20	60	100	20	60	100	20	60	100
Peak load (kN)	0.99	2.26	3.66	0.28	0.75	1.31	0.92	1.76	3.50
Adhesion strength (MPa)	-	-	-	078	2.51	3.63	0.88	1.69	2.27

Based on the presented values, it was found that the anchorage component of fibres with 3D hooks in both ends resist approximately to 72, 67 and 64% of the total load, for concretes with compressive strength of 20, 60 and 100 MPa, respectively. This shows that hooks are more important for concretes with low strengths. Moreover, the increase in concrete compressive strength leads to an increase in the number of fibres that fail, instead of debonding and slipping. This happens because fibres can easily damage the adjoining concrete matrix for lower concrete strengths, during the hook deformation process, whereas the anchorage strength between the fibre hooks and the concrete matrix is increased for matrices with higher strengths and, thus, failure of the fibres is reached before the hook starts to deform and slip.

Based on the values of Table 3 and on the results of Figures 5a and 7, evolution of bond strength with the slipping of fibres without hooks (3D1 and 5D1), it is confirmed that the peak load of specimens with 5D1 fibres is much higher than those with 3D1 fibres, due to its higher diameter and embedded length of the first, resulting on increased area of the matrix-fibres interface. However, the adhesion component of bond strength of the fibres 3D1 is about 50% higher than the corresponding value of the fibres 5D1, mainly for matrixes with strengths of 60 and 100 MPa, being similar for the matrix with 20 MPa. Considering that the friction strength is noticeable after adhesion failure, it is visible that this component first remains almost constant in the beginning of slip and then increases with the evolution of fibres slipping. For the stage with constant friction, similar values are noticeable for both 3D1 and 5D1 fibres, excepting for fibres 5D1 and matrix with 100 MPa, where the matrix strength and the fibre diameter have higher influence on friction strength, which largely exceeds the adhesion strength. The friction strength corresponds to about 70% of the adhesion, for fibres 3D1 and matrixes with 60 and 100 MPa, and for fibres 5D1 with 60 MPa of matrix strength. However,

that relation is about 30% for both fibres and matrix with 20 MPa, being of approximately 150% for fibres 5D1 and matrix with 100 MPa.

3.3.1. Numerical modelling

In order to predict the behaviour of specimens produced with different concrete mixtures, a numerical model was calibrated using the results of 3D2 set. This set was selected because it is the one adopted in construction, whereas specimens of the other test set were produced with modified fibres. The structural scheme and the corresponding finite element mesh are shown in Figure 9. The numerical model used a framework recently developed for the simulation of discrete fibres in [28]. This formulation allows embedding both fibres and strong discontinuities in regular finite element meshes, and is an alternative approach to formulations developed in [29–40]. As a particular advantage of the selected approach, it is mentioned the fact of the nodes of the fibres not being considered as global degrees of freedom (since they are embedded in the mesh) and this reduces the computational cost associated with the simulation of numerous discrete fibres. The corresponding bond-slip is taken into account using a modified constitutive law for the fibres.

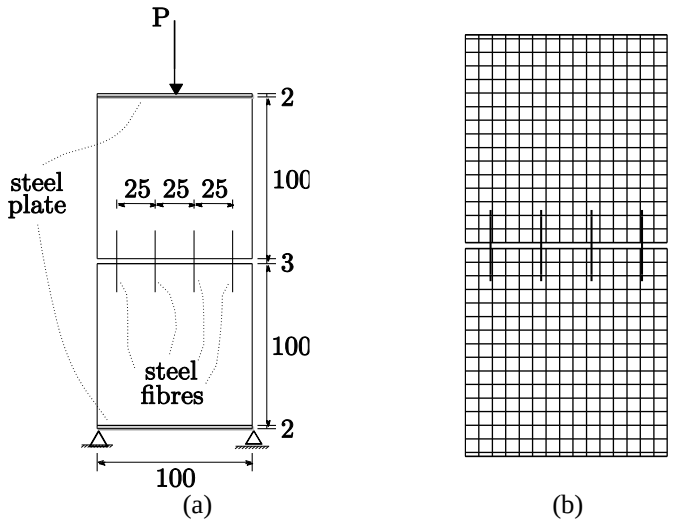

Figure 9 – 3D2 set: (a) structural scheme (dimensions in mm, 100 mm width); and (b) finite elements mesh with embedded steel fibres.

For the load level reached by the specimens, there was no need to consider the possibility of tensile fracture. Therefore, a linear elastic model assuming the Young's modulus defined in Section 2.1 was adequate to simulate concrete behaviour. Regarding the steel fibres, and following the procedure described in [28], a constitutive model that best fits the experimental results was adopted. The latter is shown in Figure 10, assuming the relevant parameters (E_1, f_{t1}, E_2, f_{t2} and E_3) different values shown in Table 4 for each concrete mixture.

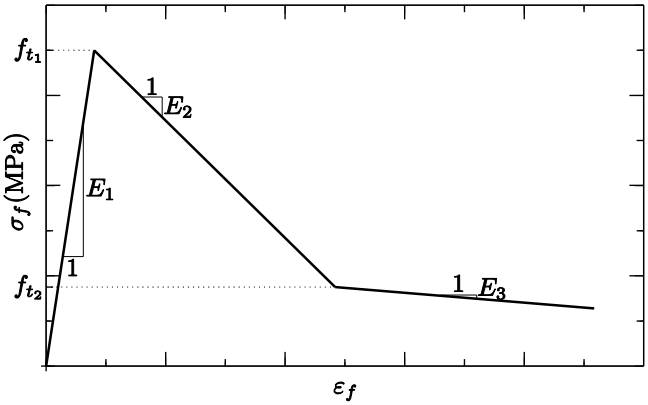

277 Figure 10 – 3D2 set: generic constitutive law for embedded steel fibres.

278

279 Table 4 – 3D2 set: values of the parameters that define the steel fibres constitutive laws for each concrete mixture.

Concrete	f_c (MPa)	E_1 (MPa)	f_{t1} (MPa)	E_2 (MPa)	f_{t2} (MPa)	E_3 (MPa)
C20	19.0	460.0	270.0	115.0	94.5	23.0
C60	64.3	2200.0	580.0	275.0	145.0	27.5
C100	100.4	5800.0	940.0	362.5	188.0	32.2

280

281 Figure 11 presents a comparison between results obtained experimentally and numerically. It can be
282 observed a good agreement for all concrete mixtures, both in terms of initial stiffness, peak load and post-
283 peak behaviour, which proves that the used fibres constitutive models are suitable to characterize the
284 behaviour of the fibre/matrix interface.

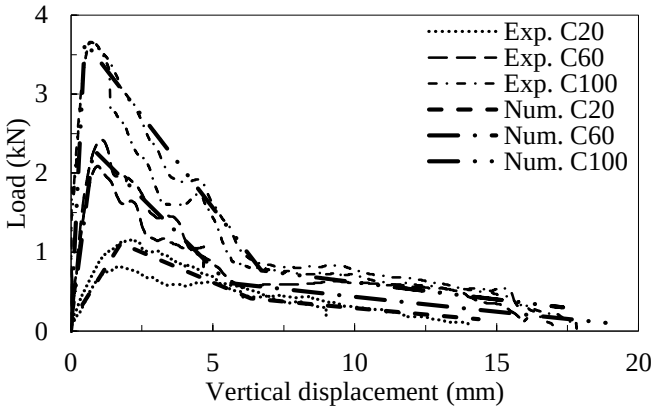

285 Figure 11 – 3D2 set: load vs. vertical displacement for all tested concrete mixtures.

286

287 In order to predict the behaviour of similar specimens made with other concretes, a regression for each
288 constitutive model parameter (dependent variable) and the concrete compressive strength (independent
289 variable) was performed. The parameters for concrete mixtures with different compressive strength were
290 successfully interpolated using a linear regression ($R^2 \geq 0.93$).

Therefore, two different constitutive models were tested in order to check the prediction given by the linear regression above described. Thus, two different concretes (C40 and C80) with compressive strength between 19.0 and 100.4 MPa were considered and the results of the parameters prediction can be observed in Table 5.

Table 5 – 3D2 set: values of the parameters obtained by linear regression.

Concrete	f_c (MPa)	E_1 (MPa)	f_{t1} (MPa)	E_2 (MPa)	f_{t2} (MPa)	E_3 (MPa)
C40	41.4	1523.8	432.4	189.3	119.4	25.3
C80	81.6	4116.2	761.0	312.4	165.6	29.8

New numerical tests were performed using the model presented in Figure 9b but considering different concretes (C40 and C80) and the respective fibre constitutive models (see Table 5). The loads vs. displacement curves, as well as the other curves obtained numerically, are shown Figure 12. It is possible to denote that the results obtained for the specimens with intermediate concrete compressive strengths are in line with the numerical results for the experimentally tested specimens, which shows the suitability of the constitutive models prediction.

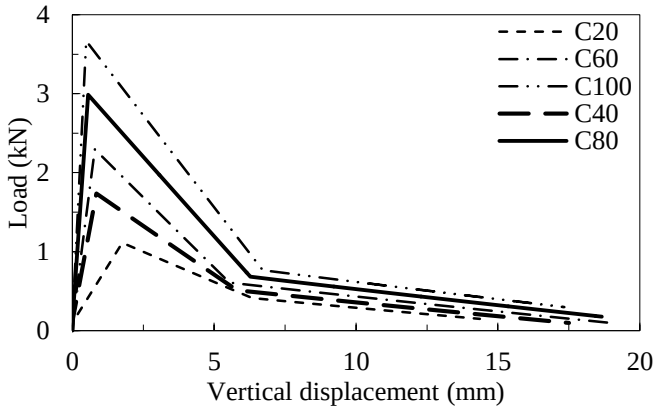

Figure 12 – 3D2 set: load vs. vertical displacement for all numerical tests.

4. Conclusions

A study focused on the influence of the concrete strength and of the steel fibres with hooked ends in the fibre/matrix interface is herein presented. The increase of concrete strength strongly influences the increase of fibre/matrix strength. Concerning the steel fibre geometry and ends configuration, different conclusions have been drawn:

- The anchorage strength of the original 3D fibres supports approximately 72% of the total strength for the matrix with 20 MPa of compressive strength, which percentage decreases for matrixes with 60 and 100 MPa of compressive strength, with respective values of 67% and 64%. This proves that the anchorage strength provided by the hooks of the fibres is more important for concrete with lower strength, being instead the bond strength less influent.

- The increase of concrete compressive strength leads to an increase in the number of original fibres that fail by tensile strength, instead of slipping and debonding of the concrete matrix. This is caused by the respective increase of interface bond strength and also by the increased difficulty of damaging the adjoining matrix during the hook deformation process.
- The peak load of specimens with 5D1 fibres is much higher than those with 3D1 fibres, due to their higher diameter and embedded length, resulting on an increased interfacial area between matrix and fibres. The adhesion component of bond strength of the fibres 3D1 is about 50% higher than the corresponding value of the fibres 5D1, mainly for matrixes with strengths of 60 and 100 MPa.
- The friction strength is noticeable after adhesion failure, increases with slip, and present similar values for both 3D1 and 5D1 fibres, excepting for fibres 5D1 and matrix with 100 MPa, where the matrix strength has higher influence on friction, which exceeds the adhesion. The friction strength corresponds to about 70% of the adhesion, for fibres 3D1 and matrixes with 60 and 100 MPa, and for fibres 5D1 with 60 MPa of matrix strength. That relation is about 30% for both fibres and matrix with 20 MPa, being 150% for fibres 5D1 and matrix with 100 MPa.

The numerical model for interfaces with 3D fibres with hooks was developed based on several parameters and correlations between the fibres and the compressive strength of the matrix. That was critical to develop suitable constitutive models that can be used for those fibres, which were calibrated using the experimental data for each matrix. The regression analysis allows predicting the constitutive model for matrixes with different compressive strengths and can be used to simulate the structural behaviour of FRC concrete members.

Acknowledgements

Authors would like to acknowledge the Portuguese Foundation for Science and Technology (FCT) by funding the project PTDC/ECM/119214/2010, entitled Concrete Behaviour at Meso-Scale, and the support through the individual grants SFRH/BD/84355/2012, SFRH/BD/85922/2012 and SFRH/BPD/102790/2014. The fifth author acknowledges the support of the Australian Research Council through the Discovery Early Career Researcher Award (DE150101703) and of the Faculty of Engineering & Information Technologies of the University of Sydney, through the Faculty Research Cluster Program. Lastly, authors acknowledge the support of the following companies that offered consumable items used in the experimental study, namely Secil, Argilis, BASF and Bekaert.

References

[1] R.S. Olivito, F.A. Zuccarello, An experimental study on the tensile strength of steel fiber reinforced concrete, Compos. Part B Eng. 41 (2010) 246–255. doi:10.1016/j.compositesb.2009.12.003.

[2] Y. Şahin, F. Köksal, The influences of matrix and steel fibre tensile strengths on the fracture energy of high-strength concrete, Constr. Build. Mater. 25 (2011) 1801–1806. doi:10.1016/j.conbuildmat.2010.11.084.

[3] V. Vairagade, K. Kene, Introduction to Steel Fiber Reinforced Concrete on Engineering Performance of Concrete, Int. J. Sci. Technol. Res. 1 (2012) 139–141.

[4] P.. Song, S. Hwang, Mechanical properties of high-strength steel fiber-reinforced concrete, Constr. Build. Mater. 18 (2004) 669–673. doi:10.1016/j.conbuildmat.2004.04.027.

[5] J. Thomas, A. Ramaswamy, Mechanical Properties of Steel Fiber-Reinforced Concrete., J. Mater. Civ. Eng. 19 (2007) 385–392. 10.1061/(ASCE)0899-1561(2007)19:5(385).

[6] N. Banthia, C. Yan, Bond-slip characteristics of steel fibers in high reactivity metakaolin (HRM) modified cement-based matrices, Cem. Concr. Res. 26 (1996) 657–662. doi:10.1016/S0008-8846(96)85000-9.

[7] M.J. Shannag, R. Brincker, W. Hansen, Pullout behavior of steel fibers from cement-based composites, Cem. Concr. Res. 27 (1997) 925–936. doi:10.1016/S0008-8846(97)00061-6.

[8] P. Robins, S. Austin, P. Jones, Pull-out behaviour of hooked steel fibres, Mater. Struct. 35 (2002) 434–442.

[9] F.U.A. Shaikh, Y. Shafaei, P.K. Sarker, Effect of nano and micro-silica on bond behaviour of steel and polypropylene fibres in high volume fly ash mortar, Constr. Build. Mater. 115 (2016) 690–698. doi:10.1016/j.conbuildmat.2016.04.090.

[10] C. DiFrancia, T.C. Ward, R.O. Claus, The single-fibre pull-out test. 1: Review and interpretation, Compos. Part A Appl. Sci. Manuf. 27 (1996) 597–612. doi:http://dx.doi.org/10.1016/1359-835X(95)00069-E.

[11] A. Bentur, S. Mindess, Fibre Reinforced Cementitious Composites, Taylor & Francis, 2007.

[12] F. Isla, G. Ruano, B. Luccioni, Analysis of steel fibers pull-out. Experimental study, Constr. Build. Mater. 100 (2015) 183–193. doi:10.1016/j.conbuildmat.2015.09.034.

[13] J.-P. Won, J.-H. Lee, S.-J. Lee, Predicting pull-out behaviour based on the bond mechanism of arch-type steel fibre in cementitious composite, Compos. Struct. 134 (2015) 633–644. doi:10.1016/j.compstruct.2015.08.127.

[14] E. Zīle, O. Zīle, Effect of the fiber geometry on the pullout response of mechanically deformed steel fibers, Cem. Concr. Res. 44 (2013) 18–24. doi:10.1016/j.cemconres.2012.10.014.

[15] A. Caggiano, H. Xargay, P. Folino, E. Martinelli, Experimental and numerical characterization of the bond behavior of steel fibers recovered from waste tires embedded in cementitious matrices, Cem. Concr. Compos. 62 (2015) 146–155. doi:http://dx.doi.org/10.1016/j.cemconcomp.2015.04.015.

[16] V.M.C.F. Cunha, J.A.O. Barros, J.M. Sena-Cruz, An integrated approach for modelling the tensile behaviour of steel fibre reinforced self-compacting concrete, Cem. Concr. Res. 41 (2011) 64–76. doi:10.1016/j.cemconres.2010.09.007.

[17] Y. Lee, S.T. Kang, J.K. Kim, Pullout behavior of inclined steel fiber in an ultra-high strength cementitious matrix, Constr. Build. Mater. 24 (2010) 2030–2041. doi:10.1016/j.conbuildmat.2010.03.009.

[18] T.S. Ng, S.J. Foster, M.L. Htet, T.N.S. Htut, Mixed mode fracture behaviour of steel fibre reinforced concrete, Mater. Struct. 47 (2014) 67–76. doi:10.1617/s11527-013-0045-1.

[19] Fédération internationale du béton., Fib model code for concrete structures 2010, n.d.

[20] EN 206-1:2013. Concrete . Part 1: Specification, performance, production and conformity., (2013).

[21] EN 934-2:2001. Admixtures for concrete, mortar and grout. Part 2: Concrete admixtures - Definitions, requirements, conformity, marking and labelling., (2001).

[22] J. Lourenço, E. Júlio, P. Maranha, Betões de Agregados Leves de Argila Expandida, APEB, 2004.

[23] E 397-1993. Betões: Determinação do módulo de elasticidade em compressão, (1993).

[24] J. Valença, E.N.B.S. Júlio, H.J. Araújo, Applications of Photogrammetry to Structural Assessment, Exp. Tech. 36 (2012) 71–81. doi:10.1111/j.1747-1567.2011.00731.x.

[25] D. Dias-da-Costa, J. Valença, E.N.B.S. Júlio, Laboratorial test monitoring applying photogrammetric post-processing procedures to surface displacements, Measurement. 44 (2011) 527–538. doi:10.1016/j.measurement.2010.11.014.

[26] J. Valença, D. Dias-da-Costa, E. Júlio, H. Araújo, H. Costa, Automatic crack monitoring using photogrammetry and image processing, Measurement. 46 (2013) 433–441. doi:10.1016/j.measurement.2012.07.019.

[27] Fédération internationale du béton., Structural concrete : textbook on behaviour, design and performance., International Federation for Structural Concrete, 2009.

[28] C. Octávio, D. Dias-da-Costa, J. Alfaiate, E. Júlio, Modelling the behaviour of steel fibre reinforced concrete using a discrete strong discontinuity approach, Eng. Fract. Mech. 154 (2016) 12–23. doi:10.1016/j.engfracmech.2016.01.006.

[29] J.E. Bolander, S. Saito, Discrete modeling of short-fiber reinforcement in cementitious composites, Adv. Cem. Based Mater. 6 (1997) 76–86. doi:http://dx.doi.org/10.1016/S1065-7355(97)90014-6.

[30] J.E. Bolander, S. Choi, S.R. Duddukuri, Fracture of fiber-reinforced cement composites: effects of fiber dispersion, Int. J. Fract. 154 (2008) 73–86. doi:10.1007/s10704-008-9269-4.

[31] M. Kunieda, H. Ogura, N. Ueda, H. Nakamura, Tensile fracture process of Strain Hardening Cementitious Composites by means of three-dimensional meso-scale analysis, Cem. Concr. Compos. 33 (2011) 956–965. doi:http://dx.doi.org/10.1016/j.cemconcomp.2011.05.010.

[32] J. Kang, J.E. Bolander, Simulating crack width distributions in SHCC under tensile loading, VIII Int. Conf. Fract. Mech. Concr. Concr. Struct. – FaMCoS-8. (2013).

[33] X. Peng, C. Meyer, A continuum damage mechanics model for concrete reinforced with randomly distributed short fibers, Comput. Struct. 78 (2000) 505–515. doi:10.1016/s0045-7949(00)00045-6.

[34] F.K.F. Radtke, A. Simone, L.J. Sluys, A computational model for failure analysis of fibre reinforced concrete with discrete treatment of fibres, Eng. Fract. Mech. 77 (2010) 597–620. doi:10.1016/j.engfracmech.2009.11.014.

[35] V.M.C.F. Cunha, J.A.O. Barros, J.M. Sena-Cruz, A finite element model with discrete embedded elements for

fibre reinforced composites, Comput. Struct. 94–95 (2012) 22–33. doi:10.1016/j.compstruc.2011.12.005.

[36] F.C. Caner, Z.P. Bažant, R. Wendner, Microplane model M7f for fiber reinforced concrete, Eng. Fract. Mech. 105 (2013) 41–57. doi:http://dx.doi.org/10.1016/j.engfracmech.2013.03.029.

[37] E. Denneman, R. Wu, E. Kearsley, A. Visser, Discrete fracture in high performance fibre reinforced concrete materials, Eng. Fract. Mech. 78 (2011) 2235–2245. doi:10.1016/j.engfracmech.2011.04.008.

[38] A. Caggiano, G. Etse, E. Martinelli, Zero-thickness interface model formulation for failure behavior of fiber-reinforced cementitious composites, Comput. Struct. 98–99 (2012) 23–32. doi:http://dx.doi.org/10.1016/j.compstruc.2012.01.013.

[39] G. Etse, A. Caggiano, S. Vrech, Multiscale failure analysis of fiber reinforced concrete based on a discrete crack model, Int. J. Fract. 176 (2012) 131–146. doi:10.1007/s10704-012-9733-z.

[40] A. Caggiano, E. Martinelli, A unified formulation for simulating the bond behaviour of fibres in cementitious materials, Mater. Des. 42 (2012) 204–213. doi:10.1016/j.matdes.2012.05.003.